Numerical simulation of resistance test for a naval vessel in shallow water

Hamidreza Mahmoodi[1], Ahmad Hajivand[2]*

[1] *BSc, Khorramshahr University of Marine Science and Technology; h.9470126@gmail.com*
[2] *2Faculty of Marine Engineering Department, Khorramshahr University of Marine Science and Technology; hajivand@kmsu.ac.ir*

ARTICLE INFO	ABSTRACT
	In this study, Computational Fluid Dynamics (CFD) computations are employed to predict the resistance, trim, sinkage, wave pattern, and bulbous bow performance of the naval model DTMB 5415 in shallow water. The simulations encompass resistance tests at various depths and velocities within the CFD environment. The impact of water depth reduction on frictional and pressure resistance components, as well as ship trimming and sinking, is assessed. A comprehensive analysis of changes in the wave pattern around the ship is conducted. Numerical results exhibit a substantial increase in resistance, trim, and sinkage with decreasing depth, highlighting the profound influence of shallow water conditions on the hydrodynamic behavior of the ship.

1. Introduction

Until about 1960, fluid dynamics was only studied using an experimental or theoretical approach. The rapid development of high-speed digital computers come along with precise numerical algorithms for solving problems. Using these computers has introduced an important third dimension to fluid dynamics, called Computational Fluid Dynamics (CFD). CFD can be applied to examine the hydrodynamics of marine vehicles especially useful in analyzing flow problems in resistance prediction where complex fluid flow is present. Among the numerous numerical techniques, Reynolds Averaged Navier Stokes (RANS) solvers that are solved by the finite volume method are today the most widely used tools for numerical prediction of ship hydrodynamic performance.

One of the most important issues in ship hydrodynamics is the prediction of its performance in shallow and restricted waters because the ship's efficiency decreases significantly with decreasing depth, such as increasing resistance, decreasing the efficiency of the propulsion system, reducing the ship's maneuverability, and so on. In addition, the probability of the ship grounding increases [1,2].

Numerous experimental and numerical researches have been done in this field. Jachowski et al. [3] simulated the resistance test in shallow water for the KCS model using a RANS solver and performed a wide assessment of ship squat. Comparison of results with the empirical method of Hooft [4] shows good accuracy of results. Pacuraru and DomniSoru predicted the hull resistance for a barge ship at different forward speed and water depth using a CFD RANS-VOF solver [5]. They concluded that increasing speed and decreasing depth greatly increases resistance. JI et al. [6] performed a numerical investigation to study the effect of ship generated waves, propeller rotational flow and current between ship and channel on sediment movement. Linde et al. [7] using ANSYS Fluent CFD software to compute resistance of an inland ship in confined waters. The results show that water depth has a greater effect on vessel strength than canal width Du et al. [8] investigated the effects of the channel dimension on resistance characteristics of two inland ships in the fully-restricted waters using numerical simulation. numerical computations of the captive maneuver tests in a shallow water condition were performed for a benchmark container ship model [9]. experimental research in shallow water shows the adverse effects of these conditions on ship maneuverability including the increase of turning diameter and the decrease of course stability [10]. Simulations of free running maneuvers for a cargo ship were conducted in shallow water also indicates the ship's worse maneuverability [11]. Tezdogan et al. predicted the ship resistance and sinkage at different ship draft at different forward speeds using numerical computations [12]. Zou et al. applied a RANS solver to consider the viscous effects and a potential flow solver to consider the free surface effects of a tanker ship advancing a channel [13].

In addition, several semi-empirical studies have been performed that suggest the effect of shallow water on resistance should be considered as a correction. One

of the first researches in this field was done by Schlichting [14]. In 2014 the ITTC [15] suggested Lackenby method [16], which was the result of a re-analysis of Schlichting.

Despite the value of these approximate relationships, today with numerical improvements, hardware capabilities and the ability to study the flow around the ship in shallow water, it is suggested to predict the hydrodynamic behavior of the ship in shallow water by performing direct simulations in CFD environment.

Bechthold and Kastens (2020) conducted a quantitative analysis of sinkage and trim for three Postpanmax containerships operating in ultra-shallow waters with a water H/T<1.2. Their study involved comparing estimated outcomes using numerical techniques to experimental fluid dynamics (EFD) for robustness assessment [17]. Song et al. (2023) investigated the impact of roughness on ship resistance and squat in shallow waters. Examining various case studies, they explored how speed and water depth contribute to the roughness penalty on ship performance [18]. The study revealed a significant influence of roughness on frictional and pressure resistance, with sinkage unaffected and trim showing substantial variation, highlighting viscous effects. Campbell et al. (2022) employed computational fluid dynamics (CFD) to analyze the effects of trim and draft on ship resistance in a narrow channel. Findings indicated that increasing an existing hull's draft raised total resistance by 10% to 15% with trim compensation, dependent on ship speed [19]. Zeng et al. (2019) calculated friction resistance for shallow-water vessels, emphasizing the impact of ship shape and water depth on model viscous resistance components [20]. The study challenged the accuracy of standard resistance extrapolation in confined waters and introduced transom effects as a novel form factor. Du et al. (2020) assessed the resistance and wave pattern of two inland ships in a fully constricted river, considering canal size, water depth, ship draft, and speed. Ship resistance was determined as a function of the blockage ratio, providing insights into the complex interplay of these factors [21]. Terziev et al. (2021) utilized a numerical RANS solver to evaluate ship effectiveness in confined water, revealing dependencies of wave-making resistance and form factor on the Reynolds number [22].

In this study, CFD computations are used to predict the Resistance, Trim, Sinkage, Wave Pattern and Bulbous Bow performance of DTMB 5415 hull with rudder in shallow water. Here, the simulation has been done for several conditions including different Froude numbers with various velocity and depth, and this research pays more attention to details which earlier studies have not. The results are compared to existing experimental ones and a good agreement is found. The results of experimental investigation are taken as a benchmark. Simulations were performed in STAR-CCM+ CFD software [23]. The study reveals that as the model moves from deep water to subcritical shallow water, there is a significant amplification in pressure resistance by up to 8 times. Simultaneously, frictional resistance experiences a fivefold increase due to increase in flow speed around the model and the wetted surface.

2. Methodology

This sector will summary the research methodology that is organized through the following key steps:
a) Goal and scope
b) Empirical methods
c) Numerical modeling

The first step states the overall purpose of the research and the scope of the analysis. In the second step, the modeling and numerical pre-processing performed to simulate the resistance test in different shallow water conditions are expressed. In the third step, the resistance tests are conducted to evaluate the ship's hydrodynamic performance. In the fourth step, the important resistance results are extracted and presented which provide a general relationship between the ship's resistance performance and water depth and forward speed.

2.1. Goal and scope

As stated previously, this paper deals with the effects of water depth on a ship's resistance performance. In this study all the resistance simulations were carried out for the DTMB 5415 model which is one of the benchmark hulls forms. The DTMB 5415 geometry was appended with a semi balanced rudder as shown in Fig. 2. The main particulars of the model-scale DTMB 5415 are listed in Table 1 [24].
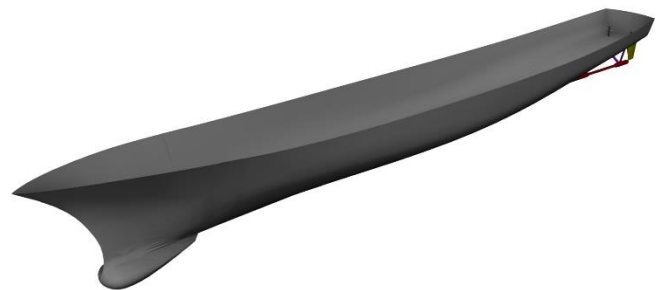

Fig 1. The DTMB 5415 geometry [24].

Table 1. Main particulars of the model-scale DTMB 5415 [24]

LBP	[m]	3.048
B	[m]	0.410
T	[m]	0.136

∇	[m3]	0.086
S	[m2]	1.371

Resistance test simulations have been performed for three different forward speeds and different depths, as shown in Table 2. This scenario focuses on the transition from low subcritical shallow water to high subcritical shallow water condition.

Table 2. Different modes of resistance test simulation

V(m/s)	0.597	0.799	0.995	1.199	1.291	1.393
Fr_h	0.281	0.376	0.469	0.564	0.608	0.656

2.2. Empirical methods

When a ship enters water of restricted depth, termed shallow water, a number of changes occur due to the interaction between the ship and the seabed. There is an effective increase in velocity, backflow, decrease in pressure under the hull and significant changes in sinkage and trim. This leads to increases in potential and skin friction drag, together with an increase in wave resistance [25].

There have been many cases of grounded ships due to squat in recent years, which are listed in Table 3. In Barass and Derrett [25], a database of more than 100 grounded ship has been collected.

Table 3. Vessels that have grounded in recent years [25]

Date	Ship name	Ship type	Location
16 Jan 2009	Mirabelle	Cargo ship	Svendborg, Denmark
20 Jan 2009	CSL Argosy	Bulk carrier	Chesapeake Bay, Baltimore
21 Jan 2009	Gunay 2	Cargo ship	Marseilles
17 Feb 2009	Ocean Nova	Cruise ship	San Martin, Antarctica
22 March 2009	Karin Schepers	Container ship	Drogden, Baltic Sound
10 June 2009	Akti N	Oil tanker	Vlissingen, Netherlands
3 April 2010	Shen Neng 1	Bulk coal carrier	Great Barrier Reef Australia
13 Aug 2010	Flinterforest	Cargo ship	Oresund Strait, Sweden
31 Jan 2011	Jack Alby 11	Trawler	Isle of Rum, Shetlands
16 Feb 2011	K-Wave	Container ship	Malaga coastline, Spain
3 Aug 2011	Karin Schepers	Container ship	St Just, near West Cornwall

There are several investigations to predict the squat in restricted water. For this purpose, Barass and Derrett [25] presented a simple formula for estimating maximum squat (in meters) in an open water condition:

$$S_{\max} = \frac{C_B \times S^{0.81} \times V_k^{2.08}}{20} \tag{1}$$

Where C_B is block coefficient, S is a blockage factor (ship cross section to the cross section of the channel ratio) and V_k is a speed in knots. Maximum squat will be at the stern if $C_B < 0.700$ and at the bow if $C_B > 0.700$. Nonetheless it is not accurate for every case.

Eryuzlu and Hausser tested the full loaded self-propelled tankers models and drew out the below formula [26]:

$$S_{BE} = 0.113B \left[\frac{1}{H/T}\right]^{0.27} Fnh^{1.8} \tag{2}$$

The above relation is for the unrestricted channels and for the squat at the bow (S_{BE}).

2.3. Numerical modelling

In this study the resistance test simulations of the DTMB 5415 were conducted using the commercial CFD software STAR-CCM+. This chapter provides details of the numerical methods applied in this paper. The turbulent unsteady viscous flow around a ship is governed by the Navier-Stokes equations. Using a RANS solver, these equations can be solved numerically and the aero-hydro dynamic forces and moments exerted to the hull, propellers and rudders are computed at each step. Based on Reynolds decomposition the averaged continuity and momentum equations for unsteady incompressible flows are given as follows [29]:

$$\frac{\partial(\rho \bar{u}_i)}{\partial x_i} = 0 \tag{3}$$

$$\frac{\partial(\rho \bar{u}_i)}{\partial t} + \frac{\partial}{\partial x_i}\left(\rho \bar{u}_i \bar{u}_j + \rho \overline{u'_i u'_j}\right) = -\frac{\partial \bar{p}}{\partial x_i} + \frac{\partial \bar{\tau}_{ij}}{\partial x_i} \tag{4}$$

where ρ indicates the fluid density, $\bar{u}_i$ indicates the averaged velocity vector, x_i (i=1, 2, 3) are the Cartesian coordinates, $\rho \overline{u'_i u'_j}$ is the Reynolds stresses, $\bar{p}$ is the mean pressure and $\bar{\tau}_{ij}$ are the mean viscous stress tensor components. This stress tensor for a Newtonian fluid can be shown in Eq. (5)

$$\bar{\tau}_{ij} = \mu \left(\frac{\partial \bar{u}_i}{\partial x_j} + \frac{\partial \bar{u}_j}{\partial x_i}\right) \tag{5}$$

in which μ means the dynamic viscosity. The Reynolds stress are approximated by turbulence models. One of the most important approaches is the use of eddy viscosity in which Reynold's tensor components are related to mean flow components.

$$-\rho \bar{u}_i \bar{u}_j = u_t \left(\frac{\partial \bar{u}_i}{\partial x_j} + \frac{\partial \bar{u}_j}{\partial x_i}\right) - \frac{2}{3}\left(\rho k + u_t \frac{\partial \bar{u}_k}{\partial x_k}\right)\delta_{ij} \tag{6}$$

where the u_t is the turbulent eddy viscosity, and k and δ_{ij} are the turbulence kinetic energy and Kronecker delta, respectively. In this numerical simulation, the two-equation SST k−ω model is used to consider the turbulence effects, which gives extremely precise predicting flow separation in the boundary layer [30]. All-y+ wall treatment is used to model the turbulent flow within the boundary layer. This model resolves RANS equations in very fine meshing conditions (y+<5), uses wall functions in coarse meshing (y+>30), and uses a blending function to calculate turbulence

quantities in the in-between y^+ [23]. Wall y^+ distribution on the hull and propeller in Fig. 2, which shows a relatively fine meshing in the boundary layer.
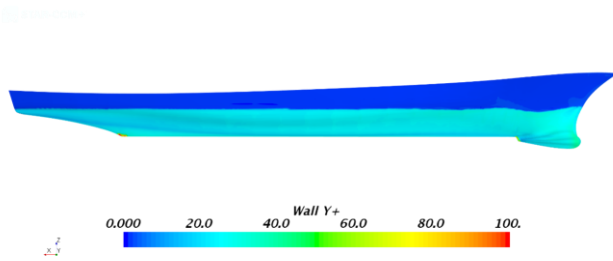

Fig. 2. Wall y^+ distribution on the hull

The highly efficient volume of fluid (VOF) technique in combination with the high-resolution-interface capturing (HRIC) scheme is applied to capture a sharp interface at the free surface between air and water.

The dynamic fluid body interaction (DFBI) method couples with RANS solver to compute the ship translations and rotations. For the current numerical simulation, the DFBI module enables the ship to move with 2 degrees of freedom including: heave and pitch to consider the dynamic trim and sinkage. At each time-step, the RSNS solver calculates the resultant forces and moments exerted the hull as well as the rudder, and with this data, the DFBI module solves the 2 DOF equations of motion and calculates the new position of the ship.

Domain was considered large enough to avoid reverse flow at outlet (2.5L from stern to outlet boundary), blockage effect due to divergent waves at wall sides(2.5L from centerline to side boundaries) Distance of domain boundaries from the hull was set according to ITTC recommendations [31]. Then, an automatic Cartesian cut-cell mesher with hexahedral base cells with trimmed cells adjacent to the surface is applied to discretize the computational domain. A surface remesher was employed to obtain a high-quality surface mesh (Fig. 3). To produce an optimal and accurate computational mesh in the areas with a high gradient at flow quantities such rudder, free surface, and around the body, a finer mesh has been created. Gradual changes in mesh size can be seen by moving away from areas with high gradients. The grids were also refined near the tight gap parts between the rudder fixed and moving parts. The obtained volume mesh is presented in Fig. 4.

Also, it is of great importance to determine appropriate boundary conditions for CFD simulations. Table 4 describes the boundary conditions of the present CFD model with the dimensions of the domain.
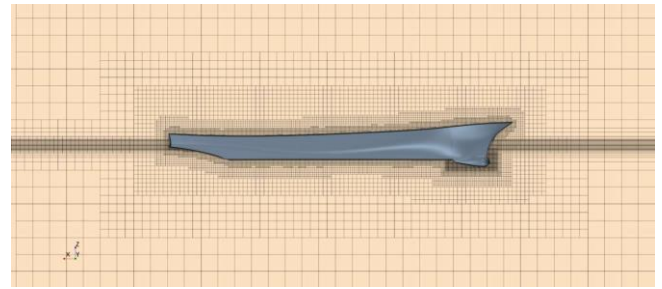

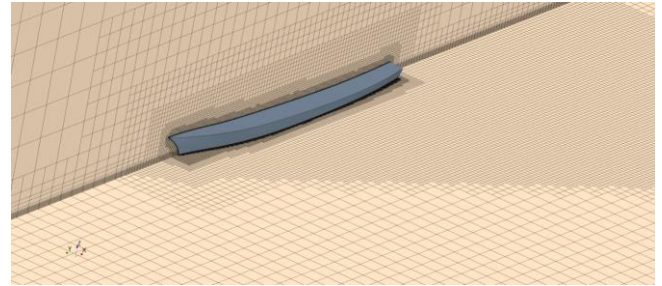**Fig. 3. Surface mesh on the hull**

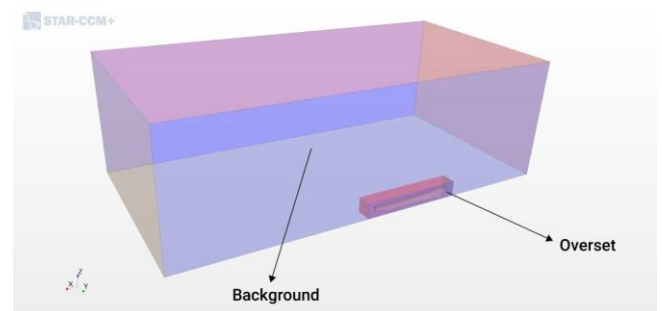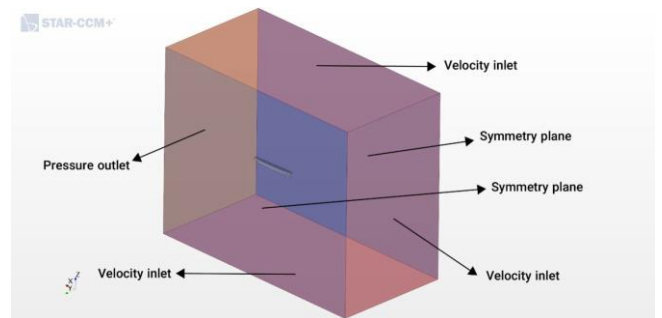**Fig. 4. Mesh distribution in the computational domain**

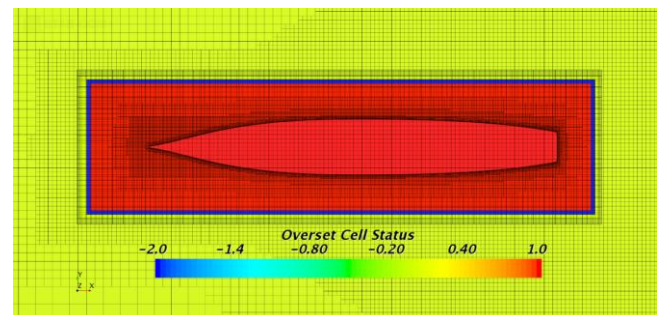**Fig. 5. Computational domain in deep and shallow water**

Fig. 6. Overset cell status around the model

Unknown quantities such as velocity and pressure were computed by the use of an unsteady implicit solver. To accelerate the convergence of the solution, an Algebraic Multigrid (AMG) algorithm was employed.

The equations of motions, flow field governing equations, and details of numerical techniques are presented in Table 4.

Table 4. Specifications of the numerical models

Governing equations	RANS
Free surface model	VOF- HRIC scheme
Turbulence model	SST k−ω
Equations of motion	DFBI (3 DOF)
Meshing model	Trimmed mesh/overset/prism layer /wall function
Solvers	FVM/unsteady implicit solver/AMG algorithm/

The time step plays a crucial role in determining the numerical stability of the results, especially when predicting the propeller revolution accurately. The time step is carefully selected to ensure that the propeller moves within a range of 0.5 to 2 degrees during each time step. based on the guidelines of ITTC the Proper time step for typical pseudo-transient resistance simulations depends on to the L/V ratio (ITTC, 2011):

$$\Delta t = 0.005 \sim 0.01 \frac{L}{V}, [s] \tag{7}$$

3. Validation and verification
3.1. Verification
the verification and validation process are performed according to the proposed procedure by ITTC to ensure the accuracy of the numerical results [32]. The verification procedure comprises classifying the errors and uncertainty create from modeling and numerical bases. Definitions of related parameters and formulas are provided in [33]. Only the verification results are presented here. The spatial and temporal discretization verification has been performed using three different cases that are successively refined with a constant refinement ratio of r= √2. To investigate the effect of time step on the accuracy and convergence of results, three simulations with different time steps (t_1,t_2,t_3) were performed for the case 2. Finally, Tables 5 and 6 compares total resistance. In these three simulations, the number of computational mesh and other variables is considered the same.

Table 5. resistance parameters for time step verification

Time step (s)	Total Resistance (N)
t_1 (0.001)	14.44
t_2 (0.0014)	14.5
t_3 (0.002)	14.6

Table 6. Time step verification

Grid Ratio	R	P	GCI
1.414	0.6	1.47	0.1125

Similarly, to study the independence of the results to the computational size, a resistance test simulation was performed for the case 2 for three different meshes (g_1, g_2, g_3). The difference in meshes in these three cases was only in the base size, and the refinement pattern was the same for all of them. The solutions obtained with g_1 (sparse mesh), g_2 (medium mesh), and g_3 (dense mesh) are designated as S_1, S_2, and S_3, respectively. The grid numbers and total resistance are presented in Table 7 and 8. And for all these quantities, the convergence parameters are calculated. The difference between the S_3 and S_2 is lower than the difference between S_2 and S_1 for all parameters. Also, the convergence ratio shows a monotonic convergence.

Table 7. resistance parameters for mesh study

Grid base size (m)	Number of Cells	Total Resistance (N)
0.0495	514392	14.44
0.07	1064858	14.6
0.1	2348252	14.9

Table 8. Mesh study verification

Grid Ratio	P	GCI
1.414	1.81	0.22

3.2. Validation

The EFD and empirical values show reasonable agreement with the CFD prediction and all results for Case 3 at the speed 0.995 m/s are illustrated and tabulated in Table 9.

Table 9. resistance validation

	Total Resistance	Error %
EFD	14.52	0.55
CFD	14.6	

4. Results and Discussion

In this section, the results obtained from numerical simulation of resistance tests in different conditions are presented.

Because an implicit unsteady solver was used, the simulations continued until the solution converged. Figure 5 shows the time history of sinkage, trim, friction and pressure resistance for case 1 (H/T=1.5). Convergence of results is well seen after the formation of a wave around the hull and the relative steadiness of the conditions.

Table 10. Total resistance at different water depth

parameters	$V\ (m/s)$	0.597	0.799	0.995	1.199	1.291	1.393
$R_t\ (N)$ in shallow water	Fr_h	0.281	0.376	0.469	0.564	0.608	0.656
	EFD	4.67	7.282	10.667	15.291	16.695	19.788
	CFD	4.58	7.3	10.98	15.9	16.87	19.92
	Error %	-1.92	0.247	2.93	3.98	1.04	0.66
$R_t\ (N)$ in deep water	EFD	3.08	5.27	8.25	12.72	14.52	16.98
	CFD	3.22	5.44	8.5	12.9	14.6	17.1
	Error %	4.54	3.22	3.03	1.415	0.55	0.7
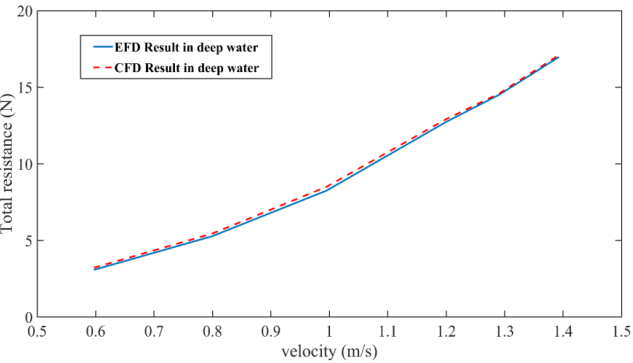
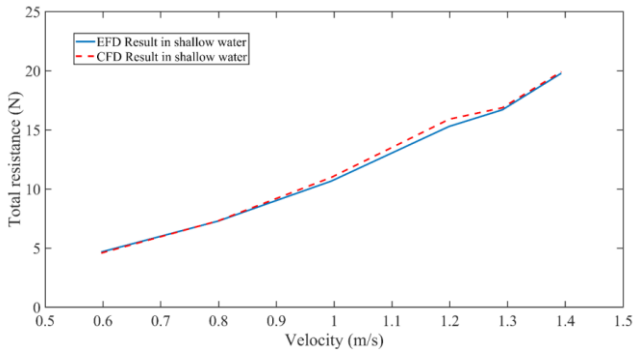Fig. 7. Total resistance validation in deep water
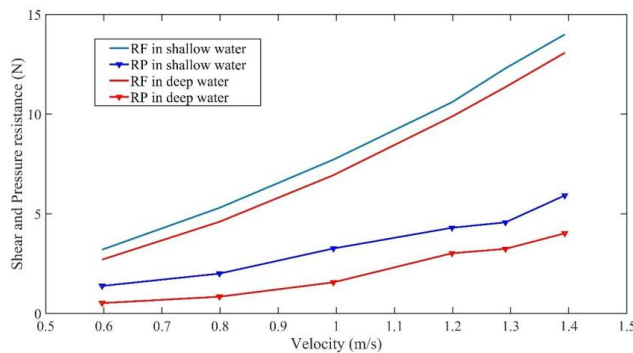

Fig. 8. Total resistance validation in shallow water

Fig. 9. Resistance components comparison in deep and shallow water

Table 11. Resistance components at different water depth

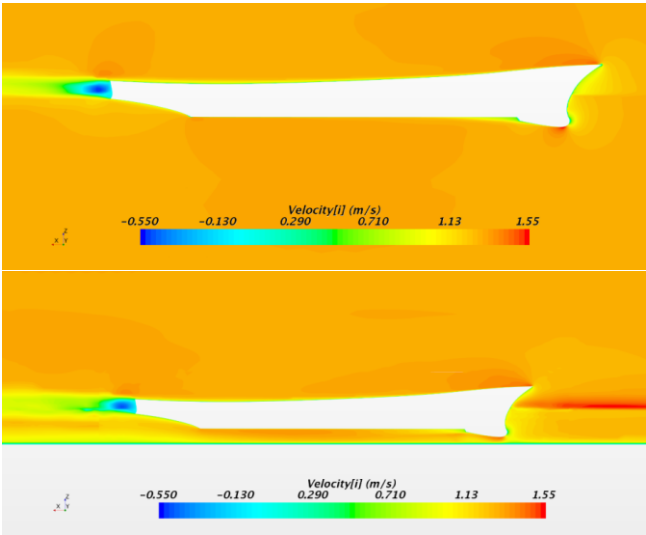| V(m/s)	CFD result in deep water			CFD result in shallow water			
	R_t	R_f	R_p	Fr_h	R_t	R_f	R_p
0.597	3.22	2.7	0.52	0.281	4.58	3.2	1.38
0.799	5.44	4.6	0.84	0.376	7.3	5.3	2
0.995	8.5	6.94	1.56	0.469	10.98	7.72	3.26
1.199	12.9	9.88	3.02	0.564	15.9	11.6	4.3
1.291	14.6	11.36	3.24	0.608	16.87	12.3	4.57
1.393	17.1	13.08	4.02	0.656	19.92	14	5.92

Fig. 10. Velocity distribution around the model; deep water (top), shallow water (bottom)
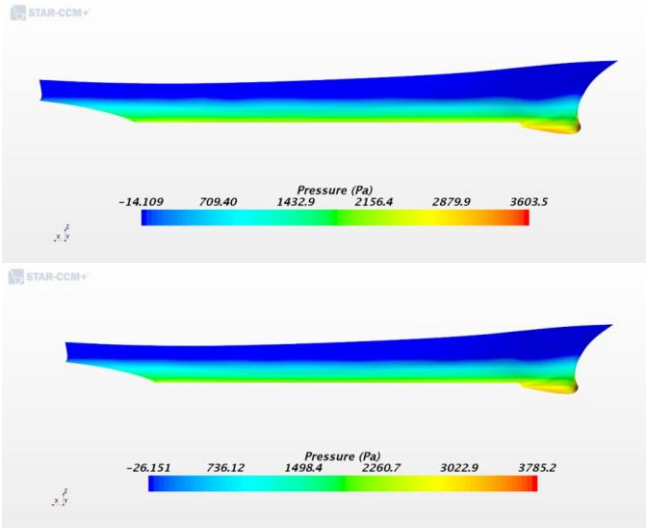

Fig. 11. Pressure distribution around the model; deep water (top), shallow water (bottom)

When a body travels through Near a free surface, the pressure variations manifest themselves by changes in the fluid level, creating waves. With a body moving through a stationary fluid, the waves travel at the same speed as the body. The overall ship wave system in deep water may be considered as being created by a number of travelling pressure points, with the Kelvin wave pattern being a reasonable representation of the actual ship wave system. However, Shallow water has significant effects on the wave pattern. At speeds well below $Fr_h = 1.0$, the wave system is as shown in Figure 7 with a transverse wave system and a divergent wave system propagating away from the ship at an angle of about 35◦. As the ship speed reaches the critical speed, $Fr_h = 1.0$, the wave angle achieves 0◦, or perpendicular to the track of the ship. At speeds greater. than the critical speed, the diverging wave system returns to a wave propagation angle of about $(\cos^{-1}(1/\ Fr_h))$, Figure 8. It can be

noted that there are now no transverse waves. Because a gravity wave cannot travel at c = √gh, the transverse wave system is left behind and now only divergent waves are present.

Similarly, it can be clearly seen that in Figure 9, which is related to Case 2, the wavelength has decreased due to the reduction in ship speed.
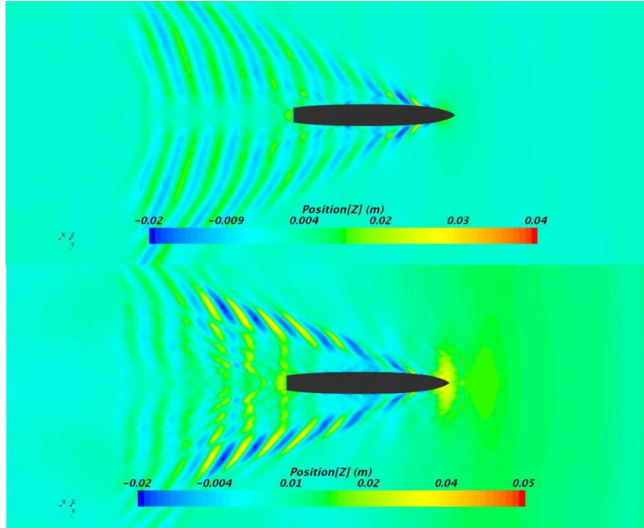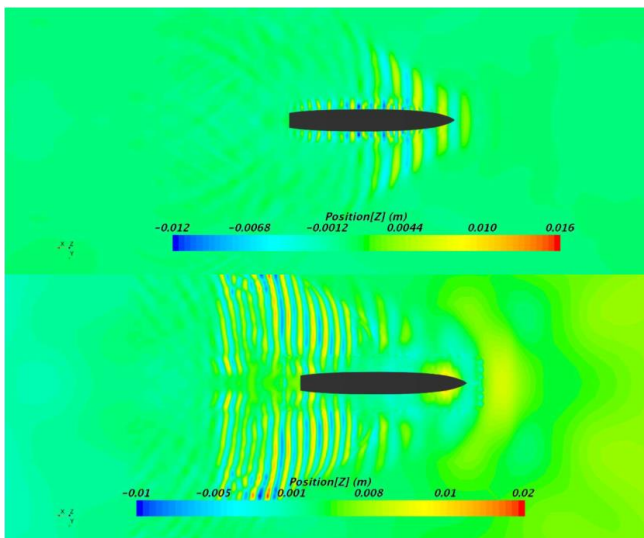

Fig. 12. The wave pattern for case 3 H/T=6

Fig. 13. The wave pattern for case 3 H/T=4 and V=2.196

It should be mention that the simulations were executed using a computer equipped with an Intel(R) Core i7 2.83GHz CPU and 16GB RAM. The final simulations, conducted on the mdium grid, achieved convergence in around 80 sec (physical time) and approximately 7 hours computational time. The convergence time extended to nearly 9 hours for Fr_h=0.656 (the shallowest case). This elongation is likely attributed to flow instabilities between the hull's bottom and the bed.

5. Conclusions
In this study, we conducted a comprehensive analysis of the effects of water depth on the total resistance, sinkage, and trim of the DTMB 5415 model through simulated experiments in both deep and shallow waters. Employing a RANS solver, our simulations were compared with empirical formulas and experimental data, revealing satisfactory accuracy. The findings underscore a notable increase in resistance, trim, and sinkage as water depth decreases. Furthermore, significant alterations in the wave pattern around the ship were observed. The findings indicated that shallow water has detrimental impacts on multiple aspects of the ship's resistance. The augmentation of wave propagation amplitude and angle, along with the amplification of pressure gradient on the hull, leads to an over speed of the flow surrounding the body, particularly beneath it. Consequently, this results in an increase in the resistance components, as well as trim and sinkage.

The hydrodynamic performance of the model exhibited a discernible disparity between the low subcritical and high subcritical flow regimes, which proved to be an intriguing observation. The impact of the rise in resistance and the decline in system efficiency becomes significantly more pronounced upon entering the zone of high subcritical flow regime.

6. References

1- Hofman, Milan & Kozarski, V. (2000). *Shallow water resistance charts for preliminary vessel design.* International Shipbuilding Progress. 47. 61-76.

2- Liu, Jialun & Hekkenberg, Robert & Rotteveel, Erik & Hopman, Hans. (2015). *Literature review on evaluation and prediction methods of inland vessel manoeuvrability.* Ocean Engineering. 106. 458-471. 10.1016/j.oceaneng.2015.07.021.

3- Jachowski, J. *Assessment of ship squat in shallow water using CFD.* Arch. Civ. Mech. Eng. 2008, 8, 27–36.

4- Hooft, J.P. *The Influence of Nautical Requirements on the Dimensions and Layout of Entrance Channels and Harbours;* Proc. International Course Modern Dredging: The Hague, The Netherlands, 1977.

5- Pacuraru, F.; Domnisoru, L. *Numerical investigation of shallow water effect on a barge ship resistance.* IOP Conf. Series Mater. Sci. Eng. 2017, 227, 012088.

6- Ji, S.; Ouahsine, A.; Smaoui, H.; Sergent, P. *3D Numerical Modeling of Sediment Resuspension Induced by the Compounding Effects of Ship-Generated Waves and the Ship Propeller.* J. Eng. Mech. 2014, 140, 04014034.

7- Linde, F.; Ouahsine, A.; Huybrechts, N.; Sergent, P. *Three-Dimensional Numerical Simulation of Ship Resistance in Restricted Waterways: Effect of Ship Sinkage and Channel Restriction.* J. Waterw. Port. Coastal. Ocean. Eng. 2017, 143, 06016003.

8- Du, P.; Ouahsine, A.; Sergent, P.; Hu, H. *Resistance and wave characterizations of inland*

vessels in the fully-confined waterway. Ocean. Eng. 2020, 210, 107580.

9- Liu, Y.; Zou, Z.; Zou, L.; Fan, S. *CFD-based numerical simulation of pure sway tests in shallow water towing tank*. Ocean. Eng. 2019, 189, 106311.

10- Xu, H.; Hinostroza, M.; Wang, Z.; Soares, C.G. *Experimental investigation of shallow water effect on vessel steering model using system identification method*. Ocean. Eng. 2020, 199, 106940.

11- Tang, X.; Tong, S.; Huang, G.; Xu, G. *Numerical investigation of the maneuverability of ships advancing in the non-uniform flow and shallow water areas*. Ocean. Eng. 2020, 195, 106679.

12- Tezdogan, T., Incecik, A., Turan, O., 2016. *A numerical investigation of the squat and resistance of ships advancing through a canal using CFD*. J. Mar. Sci. Technol. 21, 86–101.

13- Yao, J.-X., Zou, Z.-J., 2010. *Calculation of ship squat in restricted waterways by using a 3D panel method*. J. Hydrodynam. B 22, 489–494.

14- Schlichting, O. Schiffwiderstand auf beschränkter wassertiefe: *Widerstand von seeschiffen auf flachem wasser. Jahrbuch der Schiffbautechnischen Gesellschaft*; Springer: Hanburg, Germany, 1934; Volume 35, p. 127.

15- ITTC. *Speed and Power Trials, Part 2, Analysis of Speed/Power Trial Data*. In Proceedings of the 25th ITTC, Copenhagen, Denmark; 2014. Available online: https://ittc.info/media/4210/75-04-01-012.pdf

16- Lackenby, H. *The Effect of Shallow Water on Ship Speed*. Nav. Eng. J. 1964, 76, 21–26.

17- Bechthold, J., Kastens, M., 2020. *Robustness And Quality of Squat Predictions in Extreme Shallow Water Conditions Based On RANS-Calculations*. Ocean Eng. 197, 106780 Https://Doi.Org/10.1016/J.Oceaneng.2019.106780.

18- Song, Soonseok & Terziev, Momchil & Tezdogan, Tahsin & Demirel, Yigit & De Marco Muscat-Fenech, Claire & Incecik, Atilla. (2023). *Investigating Roughness Effects on Ship Resistance in Shallow Waters*. Ocean Engineering. 270. 113643. 10.1016/J.Oceaneng.2023.113643.

19- Campbell, R., Terziev, M., Tezdogan, T., Incecik, A., 2022. *Computational Fluid Dynamics Predictions of Draught and Trim Variations on Ship Resistance in Confined Waters*. Appl. Ocean Res. 126, 103301 Https://Doi.Org/10.1016/J.Apor.2022.103301.

20-Zeng, Q., Hekkenberg, R., Thill, C., 2019a. *On The Viscous Resistance of Ships Sailing in Shallow Water*. Ocean Eng. 190, 106434 Https://Doi.Org/10.1016/J. Oceaneng.2019.106434.

21- Du, P., Ouahsine, A., Sergent, P., Hu, H., 2020. *Resistance And Wave Characterizations of Inland Vessels in The Fully-Confined Waterway*. Ocean Eng. 210 Https://Doi.Org/ 10.1016/J.Oceaneng.2020.107580.

22-Terziev, M., Tezdogan, T., Incecik, A., 2021b. *A Numerical Assessment of The Scale Effects of a Ship Advancing Through Restricted Waters*. Ocean Eng. 229, 108972 Https://Doi. Org/10.1016/J.Oceaneng.2021.108972.

17- CD-adapco (2016). STAR-CCM+ 11.0 User Guide.

18- https://simman2014.dk/

19- Barrass, B. & Derrett, D.R.. (2006). *Ship Stability for Masters and Mates*. 10.1016/C2010-0-68323-4.

20-Eryuzlu, N.E. and Hausser, R. (1978). *Experimental investigation into some aspects of large vessel navigation in restricted waterways. Proceedings Symposium on Aspects of Navigability*, Delft, Netherlands, vol. 2, pp. 1–15

21- ICORELS *(International Commission for the Reception of Large Ships), Report of Working Group IV*, PIANC Bulletin No. 35, Supplement, 1980.

22- Millward, A. (1996). *A Review of the Prediction of Squat in Shallow Water*. Journal of Navigation, 49(1), 77-88. doi:10.1017/S0373463300013126

23- Ferziger, Joel & Perić, Milovan & Street, Robert. (2020). *Computational Methods for Fluid Dynamics*. 10.1007/978-3-319-99693-6.

24- Menter, Florian & Kuntz, M. & Langtry, RB. (2003). *Ten years of industrial experience with the SST turbulence model*. Heat and Mass Transfer. 4.

25- ITTC Recommended Procedures and Guidelines, 2014. *Practical guidelines for ship CFD applications*. 7.5–03 –02–03.

26- ITTC Recommended Procedures and Guidelines, 2017. *Uncertainty analysis in CFD verification and validation methodology and procedures*. 7.5-03-01-01.

27- Hasanvand, Ali & Hajivand, Ahmad & ali, Nasim. (2019). *Investigating the effect of rudder profile on 6DOF ship turning performance*. Applied Ocean Research. 92. 101918. 10.1016/j.apor.2019.101918.

28- Yun, Kunhang & Park, Byoungjae & Yeo, Dong-Jin. (2014). *Experimental Study of Ship Squat for KCS in Shallow Water*. Journal of the Society of Naval Architects of Korea. 51. 10.3744/SNAK.2014.51.1.34.